

Silicon isotope fractionation during the precipitation of quartz and the adsorption of $\text{H}_4\text{SiO}_{4(\text{aq})}$ on Fe(III)-oxyhydroxide surfaces

Hong-tao He^{1,2} · Yun Liu¹

Received: 11 April 2015 / Revised: 9 July 2015 / Accepted: 30 July 2015 / Published online: 8 August 2015
© Science Press, Institute of Geochemistry, CAS and Springer-Verlag Berlin Heidelberg 2015

Abstract Equilibrium Si isotope fractionation factors among orthosilicic acid (i.e., $\text{H}_4\text{SiO}_{4(\text{aq})}$), quartz and the adsorption complexes of $\text{H}_4\text{SiO}_{4(\text{aq})}$ on Fe(III)-oxyhydroxide surface were calculated using the full-electron wave-function quantum chemistry methods [i.e., B3LYP/6-311G(2df,p)] with a new cluster-model-based treatment. Solvation effects were carefully included in our calculations via water-droplet method combined with implicit solvent models (e.g., PCM). The results revealed that, if it is under equilibrium conditions, heavy Si isotopes would be significantly enriched in quartz in comparison to $\text{H}_4\text{SiO}_{4(\text{aq})}$. However, most of the field observations suggested that quartz would have identical or even depleted $\delta^{30}\text{Si}$ values compared to that of $\text{H}_4\text{SiO}_{4(\text{aq})}$. To explain this discrepancy between the equilibrium calculation results and the field observations, the kinetic isotope effect (KIE) associated with the formation of amorphous silica, which usually is the precursor of crystalline quartz, was investigated using quantum chemistry methods. The KIE results showed that amorphous silica would be significantly enriched in light Si isotopes during its formation. Our equilibrium fractionation results, however, matched a special type of quartz (i.e., Herkimer “diamond”) very well, due to its nearly equilibrated precipitation condition. Opposite to the case of precipitated quartz, a large equilibrium Si isotope

fractionation (i.e., -3.0 ‰) was found between the absorbed bidentate Si surface complexes (i.e., ${}^2\text{C} > \text{Fe}_2\text{O}_2\text{Si}(\text{OH})_2$) and $\text{H}_4\text{SiO}_{4(\text{aq})}$. This calculated equilibrium Si isotope fractionation factor largely differed from a previous experimental result (ca. -1.08 ‰). We found that the formation of transient or temporary surface complexes [e.g., ${}^1\text{V} > \text{Fe}_2\text{OSi}(\text{OH})_3$] may have accounted for the smaller net fractionation observed. With the equilibrium and kinetic Si isotope fractionation factors provided here, the distributions and changes of Si isotope compositions in the Earth’s surface systems can be better understood.

Keywords Si isotope · Equilibrium isotope fractionation · Kinetic isotope fractionation · Adsorption complexes · Fe(III)-oxyhydroxide · Quartz

1 Introduction

Silicon has a high crustal abundance, 27.72 %, which is only second to that of oxygen (Clarke and Washington 1924) and extensively takes part in the material cycling of spheres. Silicon has three stable isotope, ${}^{28}\text{Si}$, ${}^{29}\text{Si}$ and ${}^{30}\text{Si}$. Typically, the silicon isotope compositions of samples are expressed as the deviation (in terms of ‰) of the ratio of ${}^{30}\text{Si}/{}^{28}\text{Si}$ from the standard sample (NBS-28 or Rose Quartz), noted as $\delta^{30}\text{Si}$ { $\delta^{30}\text{Si} = [({}^{30}\text{Si}/{}^{28}\text{Si})_{\text{sample}}/({}^{30}\text{Si}/{}^{28}\text{Si})_{\text{standard}} - 1] \times 1000 \text{ ‰}$ }. Due to the recent high precision of MC-ICP-MS (superior to 0.1 ‰ $\delta^{30}\text{Si}$) and its relatively large isotopic variations, 11.8 ‰ (Opfergelt and Delmelle 2012), in Earth’s surface environments, the Si isotope compositions in many of Earth’s surface systems including soils, rivers, oceans, silicon-accumulating algae and high plants have been investigated

✉ Yun Liu
liuyun@vip.gyig.ac.cn

Hong-tao He
hehongtao0818@yeah.net

¹ State Key Laboratory of Ore Deposit Geochemistry, Institute of Geochemistry, Chinese Academy of Sciences, Guiyang 550002, China

² University of Chinese Academy of Sciences, Beijing 100049, China

(Basile-Doelsch et al. 2005; Ding et al. 2008, 2009; Georg et al. 2007, 2009; Hughes et al. 2013; Ziegler et al. 2005a, b). Comprehensive reviews of Si isotope geochemistry can be found in Opfergelt and Delmelle (2012). In general, river water and sea water have positive $\delta^{30}\text{Si}$ signals, but ground water and secondary minerals have negative ones.

Previous studies suggested that the Si isotope distribution in the Earth's surface environments resulted from the preferential release of ^{28}Si during the mineral dissolution and the preferential incorporation of ^{28}Si in the crystal lattices of secondary minerals. In fact, although light Si isotopes will be preferentially released during the dissolution, the left heavy Si isotopes will also be released into the solution as the dissolution progresses. This can eventually cause the solution to inherit the Si isotopic signals of the primary silicate minerals. Ziegler et al. (2005a) conducted dissolution experiments on basalt. The solution was initially expected to be enriched in light Si isotopes, with the trace primary minerals having been dissolved. The subsequent abrupt increase of $\delta^{30}\text{Si}$ in solution substantiates the aforementioned diagnosis. Therefore, the dissolution of primary silicate minerals probably does not cause Si isotope fractionations.

Furthermore, minerals with stronger bonds are expected to be enriched in heavy isotopes (e.g., Schauble 2004). In this case, quartz has a shorter average Si–O bond length compared to that of an aqueous H_4SiO_4 solution (1.610 vs. 1.639 Å, Hazen et al. 1989; Rastsvetaeva et al. 2009). Therefore, quartz should be enriched with ^{30}Si when it is in equilibrium with the solution, in contrast to the field observations. There must be some unknown processes to change the Si isotope compositions of quartz.

In addition, adsorption-driven Si isotope fractionation is another effect that has not been seriously investigated and may have a big impact on the Si isotope distribution in the Earth's surface environments. Because Fe(III)-oxyhydroxide is ubiquitous on the Earth's surface as a scavenger, Delstanche et al. (2009) studied the Si isotope fractionations during the adsorption of monosilicic acid onto Fe(III)-oxyhydroxide surfaces and revealed that ^{28}Si was preferentially adsorbed to the surfaces and caused about -1.08‰ fractionation in terms of $^{30/28}\text{Si}$. Silicon and germanium (Ge) have similar chemical properties. In the solution, they are both 4-coordinated species (e.g., H_4SiO_4 and H_4GeO_4). Li and Liu (2010) calculated the equilibrium Ge isotope fractionation during adsorption onto Fe(III)-oxyhydroxide surfaces and suggested a preferential adsorption of light Ge isotope with a larger isotopic fractionation (-1.7‰) than what was reported for the Si isotopes (Delstanche et al. 2009). According to Johnson et al. (2004), Si isotopes have larger relative mass differences than Ge isotopes do. It is reasonable to expect larger Si equilibrium isotopic fractionation during the adsorption of H_4SiO_4 on Fe(III)-oxyhydroxide.

In the present study, we calculated the equilibrium Si isotope fractionation factors and the possible Si kinetic isotope fractionation factors during the precipitation of quartz. Meanwhile, to check the magnitude of equilibrium Si isotopic fractionation between monosilicic acid and the adsorbed Si surface complexes on Fe(III)-oxyhydroxide surface, first-principle quantum chemistry methods were also carried out.

2 Theory and calculations

2.1 Bigeleisen and Mayer equation

Bigeleisen and Mayer (1947) and Urey (1947) established the theoretical framework of isotope geochemistry by providing the calculation method for the equilibrium constant for the isotopic exchange reaction. The central idea is about the calculation of the reduced partition function ratio (RPFR) based on the harmonic frequencies of the interested compound and its rare isotope substituted isotologue. RPFR is defined as

$$\text{RPFR} = \prod_{i=1}^{3n-6} \frac{u}{u'} \left(\frac{e^{-\frac{u}{2}}}{e^{-\frac{u'}{2}}} \right) \left(\frac{1 - e^{-u'}}{1 - e^{-u}} \right) \quad (1)$$

where $u = h\omega/kT$, with h denoting the Plank constant; k , the Boltzmann constant; T , the absolute temperature in Kelvin; c , the velocity of light; and ω , the harmonic frequencies in cm^{-1} . Readers are referred to Schauble (2004) and Liu et al. (2010) for the details of such calculation.

Given the RPFRs of a pair of compounds or minerals in equilibrium, the isotopic fractionation factor α can be derived from the ratio of their RPFRs (or β factors) if there is only one isotope substituted:

$$\alpha = \frac{\text{RPFR}_A}{\text{RPFR}_B} = \frac{\beta_A}{\beta_B} \quad (2)$$

where A and B denote different compounds or minerals. When only one isotope has been exchanged, the RPFR equals to the β isotope fractionation factor.

2.2 Kinetic isotope effect

Herein, the dimerization of the H_4SiO_4 molecules was designed to mimic the formation of amorphous silica in the Earth's surface environments. There was a large kinetic isotope effect (KIE) in the dimerization processes and therefore must be evaluated carefully. According to Bigeleisen and Wolfsberg (1958), KIE is formulated as the ratio of the rate constants of light and the heavy isotopes in the formation of the transition state complex:

$$\text{KIE} = \frac{k_L}{k_H} = \frac{\text{RPFR}_{react}}{\text{RPFR}_{ts}} \quad (3)$$

where k_L and k_H are rate constants for light and heavy isotopes, respectively, and $RPFR_{react}$ and $RPFR_{ts}$ are the reduced partition function ratios for the reactant and the transition state complex. In the calculation of $RPFR_{ts}$, one of the vibrational degrees of freedom along the path of decomposition was missing from the vibrational partition function (i.e., becomes $3n-7$). Accordingly, $RPFR_{ts}$ is in this form:

$$RPFR_{ts} = \frac{v_L^{\neq}}{v_L'^{\neq}} \prod^{3n-7} u^{\neq} \left(\frac{e^{-\frac{u^{\neq}}{2}}}{e^{-\frac{u'^{\neq}}{2}}} \right) \left(\frac{1 - e^{-u^{\neq}}}{1 - e^{-u'^{\neq}}} \right) \quad (4)$$

where v_L^{\neq} is the imaginary frequency along the path of decomposition.

2.3 Calculation methods

2.3.1 Geometry optimization of crystalline quartz

In this study, the volume variable cluster model (VVCM) method was employed in the geometry optimization and frequency calculation (Liu 2013). This method is similar to the one proposed by Rustad and co-workers (e.g., Rustad et al. 2010), but modified to improve the isotope fractionation predictions between the solids and solutions. Compared to Rustad et al.'s method, the whole cluster model of mineral now is freely optimized and the same theoretical level is used for both the solid and the solution.

To describe it in detail, the cluster model is built from three dimensional crystal structures established by X-ray diffraction or neutron diffraction data. The interested atom is located at the center of the cluster model. The dangling bonds at the edges (cutting places) is neutralized by adding virtual point charges. For example, if an O–Si bond is cut and the Si atom is removed, several positive virtual charge points will be used to substitute the Si. Their total charge will equal the charge that the removed Si had used when bonding with O (e.g., +1). Hundreds of virtual charge points were placed by surrounding the cluster model this way. Then, the cluster model's volume and geometry can be adjusted by changing the positions of the virtual charge points to search for its energy minima. All geometry optimization was implemented with the GAUSSIAN09 software package (Frisch et al. 2010). For the notoriously soft silicate structures, due to the presence of large tetrahedral member rings, geometry optimization necessitated the addition of extra polarization functions. Therefore, we employed the hybrid DFT method at the B3LYP/6-311G(2df) level to optimize the 3-dimensional structures of silicate minerals and orthosilicic acid solution, an extra set of p functions was added to this level. Finally, among cluster structures whose volumes were adjustable, the one

with the lowest energy after optimization was selected for the RPFR calculation.

The variations of the calculated average Si–O bond lengths by the VVCM method in comparison to the experimental results are given in Table 4. Specifically, the bond length errors compared to the experimental results are less than 0.5 %, while the errors of the average bond angle are less than 5 %, considerably better than other calculation methods, such as the pseudopotential based plane-wave function DFT methods.

2.3.2 Solvation effect calculation

We used a hybrid “explicit plus implicit” solvent model to simulate the solvation effects of aqueous species (e.g., orthosilicic acid) according to the suggestions from Rustad et al. (2010), i.e. a continuum solvent model was built outside the inner explicit solvent model. To construct the inner explicit solvent model, we followed the “water-droplet” method used in Liu and Tossell (2005) and Li et al. (2009) to precisely evaluate the solvation effects. An optimized initial cluster consisting of H_4SiO_4 and six water molecules continued to be optimized with an extra six water molecules until the RPFR converged to a certain value. Frequency analyses were taken to confirm that final structures of those “water-droplets” at least corresponded to the local minima of the energy. To address the effect of the different local configurations, four parallel simulations with different configurations were designed. We used this method to successfully evaluate the solvation effects in the calculation of the B, Ge and Se isotope fractionation factors (e.g., Liu and Tossell 2005; Li et al. 2009; Li and Liu 2010, 2011). Finally, water-droplet clusters with twenty-four H_2O molecules embedded in PCM-simulated solution were chosen to estimate the solvation effects of this study.

2.3.3 The structure of adsorbed Si complex on Fe(III)-oxyhydroxide surface

The results of X-ray absorption fine structure spectroscopy (XAFS) (Pokrovski et al. 2003) and ATR-IR Spectra (Swedlund et al. 2010) both indicated that the H_4SiO_4 adsorbed on the Fe(III)-oxyhydroxide was corner-sharing bidentate, i.e., ${}^2C > Fe_2O_2Si(OH)_2$. In this study, we rebuilt an edge-sharing Fe(III) octahedral dimer $[Fe_2(OH)_2(H_2O)_8]^{4+}$ according to previous studies (Li and Liu 2010 and references therein) for its excellent predicting abilities of the Ge isotopic fractionation during orthosilicic acid adsorption on Fe(III)-oxyhydroxide surfaces. The structure of this dominant edge-sharing Fe(III) octahedral dimer was experimentally confirmed by Pokrovski et al. (2003). The structure of the adsorbed Si surface complex is shown in Fig. 1 and the ground state structure has been

searched out. Comparisons of different spin multiplicity energies optimized by two bases are listed in Table 1.

Finally, we chose a corner-sharing bidentate, ${}^2\text{C} > \text{Fe}_2\text{O}_2\text{Si}(\text{OH})_2$ with a multiplicity of eleven to quantify the equilibrium Si isotopic fractionation factor between the orthosilicic acid and the adsorbed Si surface complex on the Fe(III)-oxyhydroxide.

3 Results

3.1 Determination of scaling factor

Due to the existence of anharmonicity in the experimental fundamental frequencies, we determined the scaling factor of the harmonic frequencies by comparing them with those calculated at a much higher theoretical level, such as at the B3LYP/aug-cc-PVTZ level. Table 2 shows the harmonic frequency results of several important modes of $\text{H}_4\text{SiO}_4 \cdot 6\text{H}_2\text{O}$ at different theoretical levels. Since the central silicon atom hardly moves in symmetric stretching modes, the corresponding harmonic frequencies usually do not change after the Si isotopes substitution, which means symmetric stretching modes will not contribute to the RPFR value. Therefore, we choose bending and antisymmetric stretching vibrational frequencies to determine the scaling factor. Cluster models using B3LYP/6-311G(2df,p) method can successfully predict the mid range IR adsorption frequencies, which are sensitive to the vibrational modes of Si. The calculated results are comparable to McIntosh et al. (2011) experimental data (939 cm^{-1} for antisymmetric $\nu(\text{SiO})$ stretching mode and 787 cm^{-1} for bending mode). Herein, a method of minimizing root-mean-square error (RMSE)

Table 1 The relative electronic energy differences among different spin multiplicities of ${}^2\text{C} > \text{Fe}_2\text{O}_2\text{Si}(\text{OH})_2$

	S = 9	S = 11	S = 13 (kJ/mol)
B3LYP/6-311G(d)	71 kJ/mol	0	538
B3LYP/6-311G(2df, p)	60 kJ/mol	0	554

was employed to find the best scaling factor fit (http://en.wikipedia.org/wiki/Root-mean-square_deviation; Wong 1996).

$$\text{RMSE} = \sqrt{\frac{\sum_i^N (\lambda \cdot \omega_i^{6-311G(2df,p)} - \omega_i^{\text{aug-cc-pV TZ}})^2}{N}}$$

where λ is the frequency scaling factor, $\omega_i^{6-311G(2df,p)}$ is the ith frequency calculated at B3LYP/6-311G(2df, p) level, $\omega_i^{\text{aug-cc-pV TZ}}$ is the ith frequency calculated at B3LYP/aug-cc-pV TZ level and N is the number of normal vibrational modes involved. Finally, a scaling factor of 0.98 was obtained using this method.

3.2 RPFRs of aqueous H_4SiO_4 solution

Table 3 shows the calculated RPFRs of the aqueous H_4SiO_4 of different methods. The fluctuation of RPFRs is delineated as the consequence of varied solvation effects due to the different amounts of water molecules added into the outer coordination shell (Table 3). With the increase of water molecules, the RPFR values eventually converged to a certain value (Fig. 2). Also, the hybrid method showed its effectiveness in simulating the solvation effects, evidenced by the identical RPFR value with the result of the “water droplet” method (i.e., 1.0718 vs. 1.0717) and the good results in the geometry optimization and vibrational frequency modeling (Tables 4, 5). Lastly, we used the average RPFR value (1.0718) obtained by the “water-droplet + PCM” method in later isotope fractionation calculations.

3.3 Equilibrium Si isotope fractionation between quartz and solution

Based on the calculated RPFRs, the Si isotope equilibrium fractionation between the quartz and the orthosilicic acid solution at ambient temperatures was not zero (Douthitt 1982) or a large negative value, -1.5 ‰ (Basilie-Doelsch et al. 2005), but a larger positive value about 3.3 ‰ at 298.15 K, as depicted in Fig. 3. The theoretical curve matches the observed Si isotope fractionation of euhedral quartz precipitated from the hydrothermal fluids (Dai et al. 2004, 2005; Douthitt 1982).

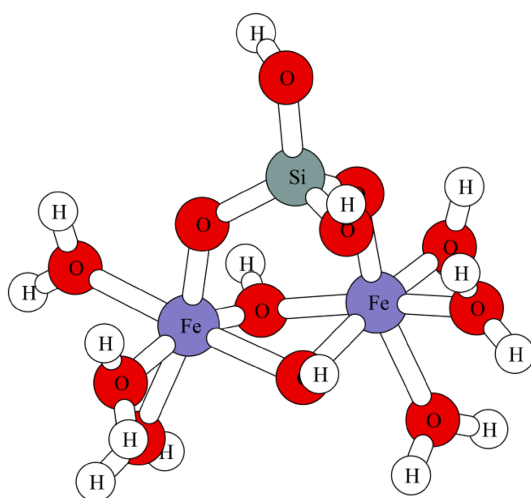


Fig. 1 The optimal structure ($S = 11$) optimized by B3LYP/6-311G(2df, p)

Table 2 Bending and antisymmetric stretching harmonic frequencies calculated by different theoretical levels

Bases	Harmonic frequencies (cm^{-1})					
	Bending modes			Antisymmetric stretching modes		
B3LYP/6-311G(2df,p) (original)	410.10	435.00	447.38	880.81	951.27	989.28
B3LYP/6-311G(2df,p) (0.98)	401.90	426.30	438.43	863.20	932.25	969.50
B3LYP/aug-cc-pVTZ	403.00	408.44	442.89	901.50	920.62	967.36

Table 3 Calculated RPFRs of aqueous H_4SiO_4 of different methods

Clusters	RPFR ^a (298.15 K)	RPFR ^b (298.15 K)
Conformer_A_ $\text{H}_4\text{SiO}_4\text{-}(\text{H}_2\text{O})_6$	1.07446	1.07198
Conformer_B_ $\text{H}_4\text{SiO}_4\text{-}(\text{H}_2\text{O})_6$	1.07438	1.07191
Conformer_C_ $\text{H}_4\text{SiO}_4\text{-}(\text{H}_2\text{O})_6$	1.07456	1.07208
Conformer_D_ $\text{H}_4\text{SiO}_4\text{-}(\text{H}_2\text{O})_6$	1.07429	1.07182
Average	1.07442	1.07195
Conformer_A_ $\text{H}_4\text{SiO}_4\text{-}(\text{H}_2\text{O})_{12_C}$	1.07351	1.07107
Conformer_B_ $\text{H}_4\text{SiO}_4\text{-}(\text{H}_2\text{O})_{12_C}$	1.07401	1.07155
Conformer_C_ $\text{H}_4\text{SiO}_4\text{-}(\text{H}_2\text{O})_{12_B}$	1.07394	1.07148
Conformer_D_ $\text{H}_4\text{SiO}_4\text{-}(\text{H}_2\text{O})_{12_B}$	1.07385	1.07139
Average	1.07383	1.07137
Conformer_A_ $\text{H}_4\text{SiO}_4\text{-}(\text{H}_2\text{O})_{18_C}$	1.07428	1.07181
Conformer_B_ $\text{H}_4\text{SiO}_4\text{-}(\text{H}_2\text{O})_{18_B}$	1.07416	1.07169
Conformer_C_ $\text{H}_4\text{SiO}_4\text{-}(\text{H}_2\text{O})_{18_C}$	1.07368	1.07123
Conformer_D_ $\text{H}_4\text{SiO}_4\text{-}(\text{H}_2\text{O})_{18_B}$	1.07447	1.07200
Average	1.07415	1.07168
Conformer_A_ $\text{H}_4\text{SiO}_4\text{-}(\text{H}_2\text{O})_{24_C}$	1.07405	1.07159
Conformer_B_ $\text{H}_4\text{SiO}_4\text{-}(\text{H}_2\text{O})_{24_B}$	1.07394	1.07148
Conformer_C_ $\text{H}_4\text{SiO}_4\text{-}(\text{H}_2\text{O})_{24_C}$	1.07420	1.07174
Conformer_D_ $\text{H}_4\text{SiO}_4\text{-}(\text{H}_2\text{O})_{24_B}$	1.07429	1.07182
Average	1.07412	1.07166
Preferred value	1.0741	1.0717
Conformer_A_ $\text{H}_4\text{SiO}_4\text{-}(\text{H}_2\text{O})_{24_C_PCM}$	1.07173	
Conformer_B_ $\text{H}_4\text{SiO}_4\text{-}(\text{H}_2\text{O})_{24_B_PCM}$	1.07153	
Conformer_C_ $\text{H}_4\text{SiO}_4\text{-}(\text{H}_2\text{O})_{24_C_PCM}$	1.07201	
Conformer_D_ $\text{H}_4\text{SiO}_4\text{-}(\text{H}_2\text{O})_{24_B_PCM}$	1.07207	
Average	1.0718	

The bold values are preferred ones

^a Data were calculated at B3LYP/6-311 g(2df, p) level

^b Data were calculated at B3LYP/6-311 g(2df, p) level, with a scaling factor 0.98

3.4 KIE in the dimerization process of orthosilicic acid

The stable reactant and product are depicted in Fig. 4. A transition-state complex with a five-coordinated Si was identified using the synchronization transition quasi-Newton searching methods (i.e., the QST3 method in Gaussian 09). Our previous study showed that either the polymerization or the depolymerization processes of quartz would be extremely difficult, even with the help of electrolytes and H^+ or OH^- ion (Zhang and Liu 2014). The activation energy calculation here shows a higher energy barrier of

135 kJ/mol for the dimerization of H_4SiO_4 molecules, which is in agreement with previous works (McIntosh 2012; Nangia and Garrison 2008; Zhang and Liu 2014) (Fig. 4). Moreover, the calculated KIE value of 1.005 suggests that the light Si isotopes were enriched in the transition-state complex, then in the product.

3.5 Si isotope fractionation during H_4SiO_4 adsorption on Fe(III)-oxyhydroxide surface

The optimized structures of aqueous ${}^{23}\text{Si} > \text{Fe}_2\text{O}_2\text{Si(OH)}_2$ are shown in Fig. 5 and Table 4. Equilibrium Si isotope

fractionations predicted by the models with two or four water molecules are slightly different (Table 6). However, their average results are the same. It means the change of solvation effects will be small if there are already four water molecules around the adsorption complex (Fig. 5). Therefore, our Si equilibrium isotope fractionation results

should be close to the true value. The average $1000\ln(\alpha)$ is -3.0 ‰ , about three times of the value (-1.08 ‰) as determined by Delstanche et al. (2009).

4 Discussion

4.1 Si isotope fractionation between quartz and solution

The equilibrium Si isotope fractionation between the quartz and the orthosilicic acid solution predicted here is largely different from the field observations (e.g., Basile-Doelsch et al. 2005; Heck et al. 2011; van den Boorn et al. 2010). Because the average Si–O bond length in quartz is much shorter than that in aqueous H_4SiO_4 (i.e., 1.610 vs. 1.639 Å) (Hazen et al. 1989; Rastsvetaeva et al. 2009), the equilibrium Si isotope fractionation between these two compounds should not be as most of the field observations suggested. The kinetic isotope effect during the formation of quartz may be the cause of such offset.

Usually, an amorphous silica precursor is formed before the formation of final crystalline quartz. In the above KIE

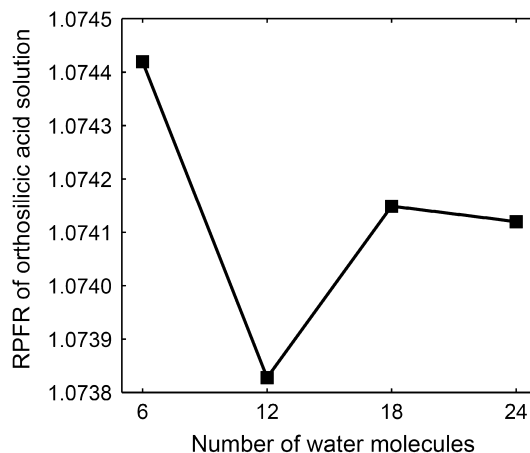


Fig. 2 RPFR values of aqueous H_4SiO_4 calculated at B3LYP/6-311G (2df, p) level

Table 4 Average Si–O bond length of optimized H_4SiO_4 solution, adsorbed Si surface complexes and quartz

Configurations	Aver. Si–O bond length (Å)	Exp. Si–O bond length* (Å)
Conformer_A_H ₄ SiO ₄ -(H ₂ O) ₂₄ _C_PCM	1.637	–
Conformer_B_H ₄ SiO ₄ -(H ₂ O) ₂₄ _B_PCM	1.638	–
Conformer_C_H ₄ SiO ₄ -(H ₂ O) ₂₄ _C_PCM	1.635	–
Conformer_D_H ₄ SiO ₄ -(H ₂ O) ₂₄ _B_PCM	1.635	–
Aver. Si–O bond length in H_4SiO_4 solution	1.636	1.639
>Fe ₂ O ₂ Si(OH) ₂ (² C)-(H ₂ O) ₂ _pcm_a	1.638	–
>Fe ₂ O ₂ Si(OH) ₂ (² C)-(H ₂ O) ₂ _pcm_b	1.640	–
>Fe ₂ O ₂ Si(OH) ₂ (² C)-(H ₂ O) ₄ _pcm_a	1.637	–
>Fe ₂ O ₂ Si(OH) ₂ (² C)-(H ₂ O) ₄ _pcm_b	1.640	–
Aver. Si–O bond length of bidentate	1.639	–
>Fe ₂ OSi(OH) ₃ (¹ V)-(H ₂ O) ₅ _a_pcm	1.634	–
>Fe ₂ OSi(OH) ₃ (¹ V)-(H ₂ O) ₅ _b_pcm	1.639	–
Aver. Si–O bond length of monodentate	1.637	–
Quartz	1.610	1.613

Experimental data are from Hazen et al. (1989) and Rastsvetaeva et al. (2009)

Table 5 Comparisons of modeled antisymmetric v (SiO) stretching mode and symmetric v (SiO) stretching mode with experimental data (McIntosh et al. 2011)

Configurations	Antisymmetric v (SiO) (cm ⁻¹)	Symmetric v (SiO) (cm ⁻¹)
Conformer_A_H ₄ SiO ₄ -(H ₂ O) ₂₄ _C_PCM	942	781
Conformer_B_H ₄ SiO ₄ -(H ₂ O) ₂₄ _B_PCM	938	776
Conformer_C_H ₄ SiO ₄ -(H ₂ O) ₂₄ _C_PCM	930	792
Conformer_D_H ₄ SiO ₄ -(H ₂ O) ₂₄ _B_PCM	928	781
Aver.	935	783
Exp.	939	787

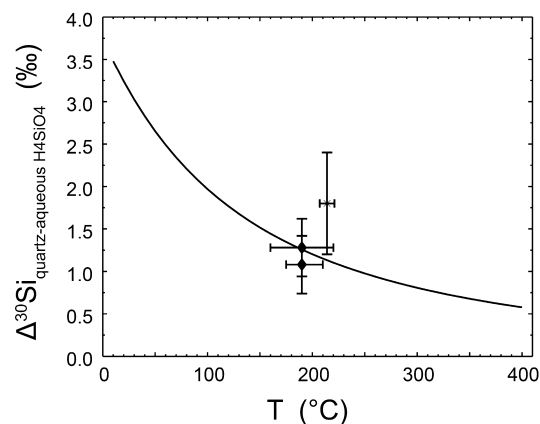


Fig. 3 Theoretical Si isotope equilibrium fractionation between quartz and aqueous H_4SiO_4 solution. Experimental data are from Douthitt (1982) (star), Dai et al. (2004, 2005) (diamond). The curve is the results of this study

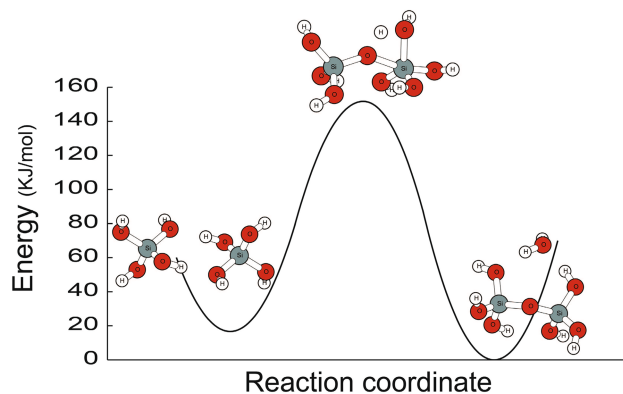


Fig. 4 The transition state complex and activation energy for $\text{H}_4\text{SiO}_4 + \text{H}_4\text{SiO}_4$ dimerization process, at B3LYP/6-311 + G(2df,p) level and with solvation effects of PCM method

calculation, we find that the KIE associated with the formation of a dimer of H_4SiO_4 , i.e., an amorphous silica precursor analogue, can let its $\delta^{30}\text{Si}$ decrease about 5 ‰ at room temperature, suggesting that the final crystalline quartz can have very light Si isotope compositions, if it inherits light Si isotope signals from its amorphous precursor. Note that the 5 ‰ enrichment of light Si isotope is just for the KIE of a single-step polymerization process. The field observations are the final results of multi-steps and multi-causes. It is not reasonable to expect a perfect match between them.

However, a special kind of quartz, the so-called Herkimer “diamond,” which is extremely pure, is thought to be precipitated under an equilibrium condition. Okamoto and Tsuchiya (2009) suggested that this kind of quartz must be slowly grown in an upward fluid flow to form such a special double-terminated crystal. This also implies a huge solution reservoir for it (e.g., ruling out isotope reservoir effect). The known Si isotopic composition of the

Herkimer diamond is very “heavy” and its $\delta^{30}\text{Si}$ value is +1.4 ‰ (Rose Quartz as standard sample), which is +1.8 ‰ heavier than the coexisting hydrothermal fluid (Douthitt, 1982). Our equilibrium fractionation result is in good consistence with the result of this special type of quartz (Fig. 2). Another line of evidence is that the veined quartzes in the two coal seams precipitated from the low-temperature hydrothermal fluids had positive a Si isotopic composition: $\delta^{30}\text{Si} = +0.4$ ‰ and $+0.6$ ‰ (Dai et al., 2004, 2005). Their results are in line with our equilibrium isotope fractionation calculation (Fig. 3). Therefore, if quartz is precipitated at equilibrium or near equilibrium conditions, its Si isotope signals will be close to our prediction. Otherwise, the kinetic isotope effects in the amorphous quartz formation processes play the role.

4.2 Si isotope fractionation during H_4SiO_4 adsorption on Fe(III)-oxyhydroxide surface

It is suspected that the equilibrium Si isotope fractionation during the adsorption on Fe(III)-oxyhydroxide surfaces determined by experiments possibly cannot represent the equilibrium fractionation value. The experimental results may be affected by the adsorption of unstable Si-surface complexes. To verify our speculation, the Si isotope fractionation between aqueous monodentate $^1\text{V} > \text{Fe}_2\text{OSi(OH)}_3$ (Fig. 6) and aqueous H_4SiO_4 was carefully investigated. We found a relatively smaller Si equilibrium isotope fractionation –1.1 ‰ (Table 7) compared to the stable bidentate surface complexes. This much smaller fractionation matched the experimental results very well. Therefore, the Si isotope fractionation results obtained in Delstanche et al. (2009) and Geilert et al. (2014) could possibly represent a result for those transient Si isotope exchanges, where the adsorbed Si complexes were only monodentates, instead of stable bidentates. A longer experiment time is definitely needed to clarify this issue in future.

5 Conclusion

The newly proposed VVCM method is used to calculate several important equilibrium Si isotope fractionation factors among quartz, adsorbed Si on Fe(III)-oxyhydroxide surface and the H_4SiO_4 solution at a decent theoretical level [i.e., B3LYP/6-311G(2df,p)]. The quartz can be enriched with heavier Si isotopes than the H_4SiO_4 solution if it is at equilibrium, up to 3.3 ‰. Most of the field observations, except euhedral quartz of hydrothermal origin, did not match our calculations for the equilibrium conditions. On the contrary, our KIE calculation results suggested that the light Si isotope enrichment of the field observed quartz was caused by the large kinetic isotope

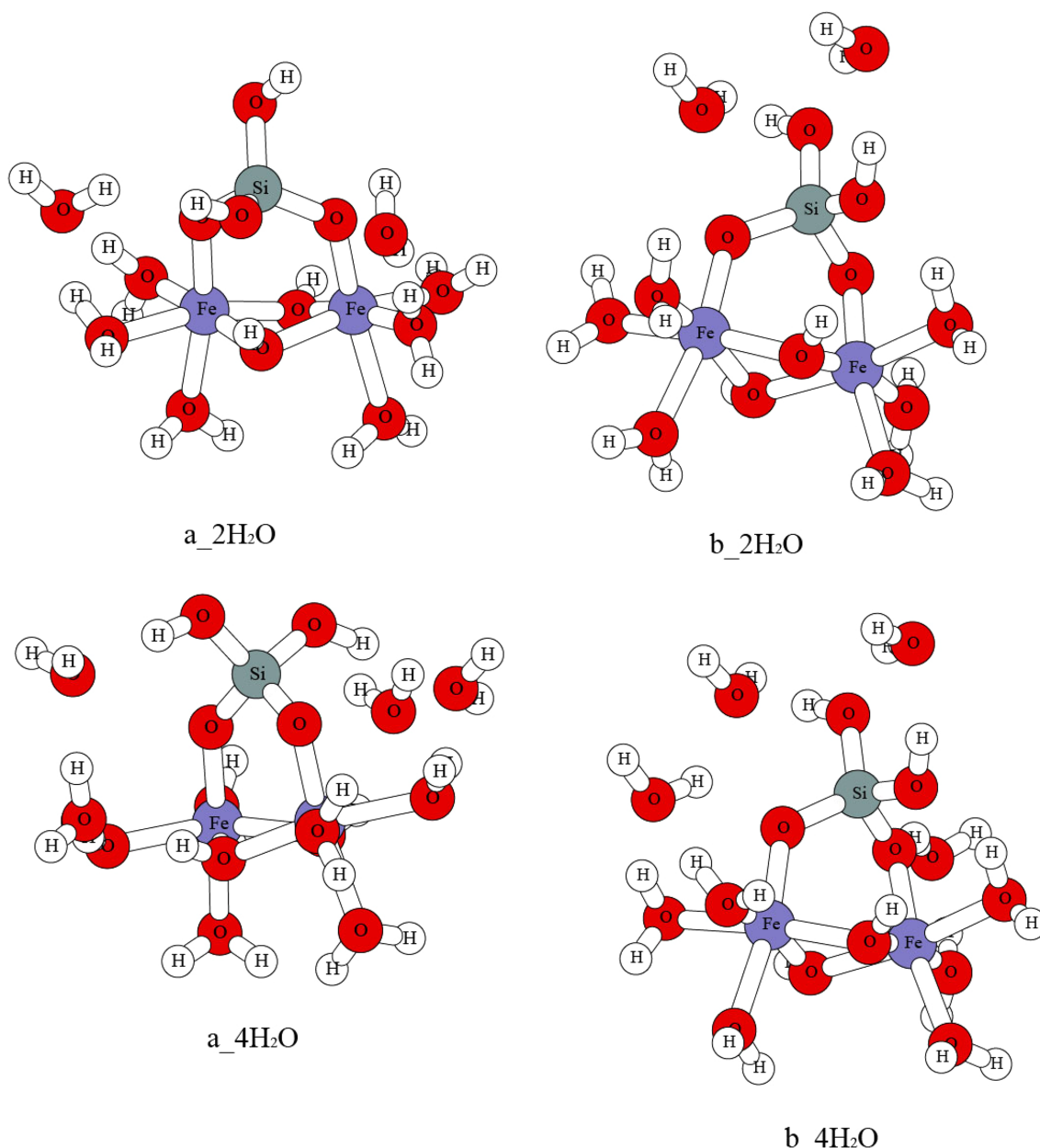


Fig. 5 Optimized structures of aqueous $^{2}\text{C} > \text{Fe}_2\text{O}_2\text{Si}(\text{OH})_2$ at B3LYP/6-311G (2df, p) level

Table 6 Silicon equilibrium isotope fractionation between aqueous $^{2}\text{C} > \text{Fe}_2\text{O}_2\text{Si}(\text{OH})_2$ and H_4SiO_4 solution with two or four water molecules nearby

Absorbates	RPFR (25 °C)	1000ln(α) _{absorbate-solution (%)}
> $\text{Fe}_2\text{O}_2\text{Si}(\text{OH})_2(^2\text{C})-(\text{H}_2\text{O})_2$ _pcm_a	1.06900	-2.6
> $\text{Fe}_2\text{O}_2\text{Si}(\text{OH})_2(^2\text{C})-(\text{H}_2\text{O})_2$ _pcm_b	1.06815	-3.4
> $\text{Fe}_2\text{O}_2\text{Si}(\text{OH})_2(^2\text{C})-(\text{H}_2\text{O})_4$ _pcm_a	1.06881	-2.8
> $\text{Fe}_2\text{O}_2\text{Si}(\text{OH})_2(^2\text{C})-(\text{H}_2\text{O})_4$ _pcm_b	1.06842	-3.2
Average	1.06860	-3.0

effect associated with the formation of amorphous quartz precursor. Meanwhile, the stable absorption surface complexes of $\text{H}_4\text{SiO}_4\text{(aq)}$ on Fe(III)-oxyhydroxide surfaces were

determined and a large equilibrium Si isotope fractionation ($\sim -3.0 \text{ } \text{\textperthousand}$) was found between the adsorbates and the H_4SiO_4 solution, which considerably differed from the

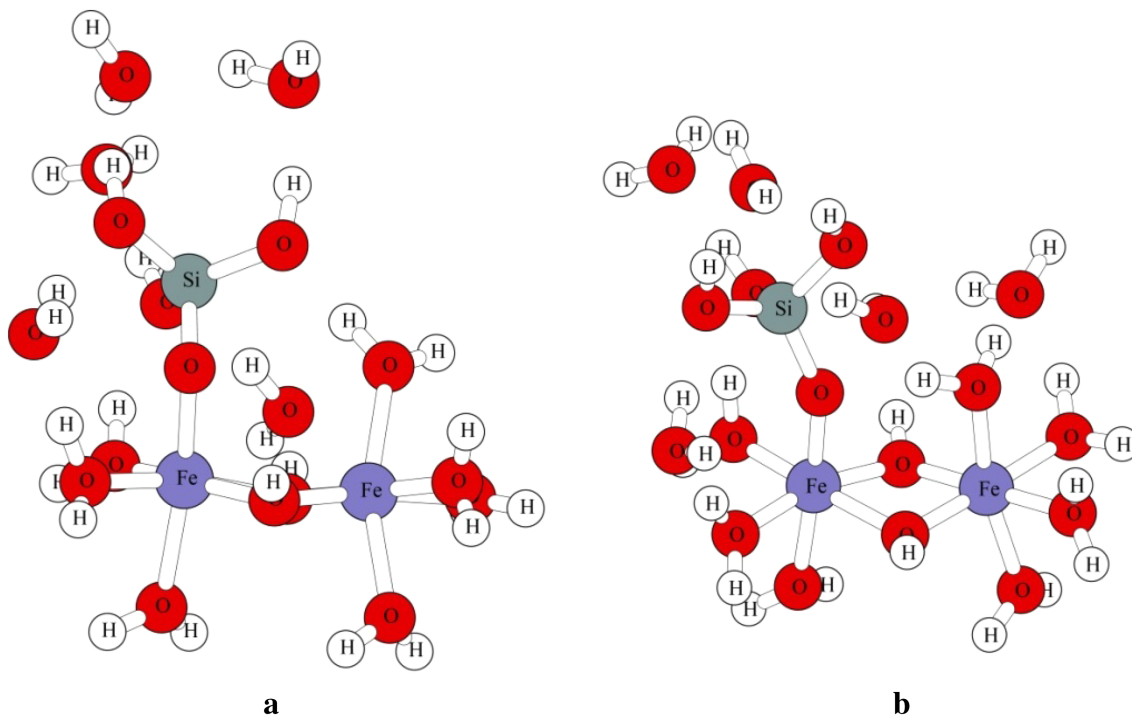


Fig. 6 Optimized structures of aqueous $^{1}\text{V} > \text{Fe}_2\text{OSi(OH)}_3$ at B3LYP/6-311G (2df, p) level

Table 7 RPFR values and silicon equilibrium isotope fractionation between aqueous $^{1}\text{V} > \text{Fe}_2\text{OSi(OH)}_3$ and H_4SiO_4 solution

Absorbates	RPFR (25 °C)	1000ln(α) _{absorbate-solution (%)}
> $\text{Fe}_2\text{OSi(OH)}_3(^1\text{V})-(\text{H}_2\text{O})_5\text{-a_pcm}$	1.07107	-0.7
> $\text{Fe}_2\text{OSi(OH)}_3(^1\text{V})-(\text{H}_2\text{O})_5\text{-b_pcm}$	1.07022	-1.5
Average	1.07065	-1.1

experimental results. Because the transient monodentate adsorption complexes have a Si isotope fractionation very close to the experimental results, we doubt that the experiments were conducted in a quick way, so that the stable bidentate adsorbates even did not have time to form.

Acknowledgments We are grateful for funding support from the 973 Program (2014CB440904) and the Chinese NSF projects (41490635, 41173023, 41225012). We thank Prof. Chen Zhu (Indiana University) for the helpful discussion.

References

- Basile-Doelsch I, Meunier JD, Parron C (2005) Another continental pool in the terrestrial silicon cycle. *Nature* 433:399–402
- Becke AD (1993) A new mixing of hartreee-fork and local density-functional theories. *J Chem Phys* 98:1372–1377
- Bigeleisen J, Mayer MG (1947) Calculation of equilibrium constants for isotopic exchange reactions. *J Chem Phys* 15:261–267
- Bigeleisen J, Wolfsberg M (1958) Theoretical and experimental aspects of isotope effects in chemical kinetics. *Advance in Chemical Physics*. 1:15–76
- Clarke FW, Washington HS (1924) The composition of the Earth's crust. United States Geological Survey Professional Paper 127
- Dai S, Li D, Ren D, Tang Y, Shao L, Song H (2004) Geochemistry of the late Permian No. 30 coal seam, Zhijin Coalfield of Southwest China: influence of a siliceous low-temperature hydrothermal fluid. *Appl Geochem* 19:1315–1330
- Dai S, Chou C-L, Yue M, Luo K, Ren D (2005) Mineralogy and geochemistry of a Late Permian coal in the Dafang Coalfield, Guizhou, China: influence from siliceous and iron-rich calcic hydrothermal fluids. *Int J Coal Geol* 61:241–258
- Delstanche S, Opfergelt S, Cardinal D, Elsass F, André L, Delvaux B (2009) Silicon isotopic fractionation during adsorption of aqueous monosilicic acid onto iron oxide. *Geochemica et Cosmochimica Acta* 73:923–934
- Ding T, Tian S, Sun L, Wu L, Zhou J, Chen Z (2008) Silicon isotope fractionation between rice plants and nutrient solution and its significance to the study of the silicon cycle. *Geochemica et Cosmochimica Acta* 72:5600–5615
- Ding T, Zhou J, Wan D, Chen Z, Wang C, Zhang F (2009) Silicon isotope fractionation in bamboo and its significance to the biogeochemical cycle of silicon. *Geochemica et Cosmochimica Acta*. 72:1381–1395
- Douthitt C (1982) The geochemistry of the stable isotopes of silicon. *Geochemica et Cosmochimica Acta* 46:1449–1458
- Frisc MJ, Trucks GW, Schlegel HB, Scuseria GE, Robb MA, Cheeseman JR, Scalmani G, Barone V, Mennucci B, Petersson GA, Nakatsuji H, Caricato M, Li X, Hratchian HP, Izmaylov AF, Bloino J, Zheng G, Sonnenberg JL, Hada M, Ehara M, Toyota K, Fukuda R, Hasegawa J, Ishida M, Nakajima T, Honda Y, Kitao

- O, Nakai H, Vreven T, Montgomery JA, Peralta Jr JE, Ogliaro F, Bearpark M, Heyd JJ, Brothers E, Kudin KN, Staroverov VN, Keith T, Kobayashi R, Normand J, Raghavachari K, Rendell A, Burant JC, Iyengar SS, Tomasi J, Cossi M, Rega N, Millam JM, Klene M, Knox JE, Cross JB, Bakken V, Adamo C, Jaramillo J, Compers R, Stratmann RE, Yazyev O, Austin AJ, Cammi R, Pomelli C, Ochterski JW, Martin RL, Morokuma K, Zakrzewski VG, Voth GA, Salvador P, Dannenberg JJ, Dapprich S, Daniels AD, Farkas O, Foresman JB, Ortiz JV, Cioslowski J, Fox DJ (2010) Gaussian 09 (Revision C.01). Gaussian, Inc., Wallingford
- Geilert S, Vroon PZ, Roerdink DL, Van Cappellen P, van Bergen MJ (2014) Silicon isotope fractionation during abiotic silica precipitation at low temperature: Inferences from flow-through experiments. *Geochemica et Cosmochimica Acta* 142:95–114
- Georg R, Reynolds B, West A, Burton K, Halliday A (2007) Silicon isotope variations accompanying basalt weathering in Iceland. *Earth Planet Sci Lett* 261:476–490
- Georg R, Zhu C, Reynolds B, Halliday A (2009) Stable silicon isotopes of groundwater, feldspars, and clay coatings in the Navajo Sandstone aquifer, Black Mesa, Arizona, USA. *Geochemica et Cosmochimica Acta* 73:2229–2241
- Hazen R, Finger L, Hemley R, Mao H (1989) High-pressure crystal chemistry and amorphization of α -quartz. *Solid State Commun* 72:507–511
- Heck PR, Huberty JM, Kita NT, Ushikubo T, Kozdon R, Valley JW (2011) SIMS analyses of silicon and oxygen isotope ratios for quartz from Archean and Paleoproterozoic banded iron formations. *Geochemica et Cosmochimica Acta* 75:5879–5891
- Hughes H, Sondag F, Santos R, André L, Cardinal D (2013) The riverine silicon isotope composition of the Amazon Basin. *Geochemica et Cosmochimica Acta*. 121:637–651
- Johnson CM, Beard BL, Albarède F (2004) Geochemistry of non-traditional stable isotopes. *Rev Miner Geochem* 55:1–24
- Li XF, Liu Y (2010) First-principle study of Ge isotope fractionation during adsorption onto Fe(III)-oxyhydroxide surfaces. *Chem Geol* 278:15–22
- Li XF, Liu Y (2011) Equilibrium Se isotope fractionation parameters: a first-principles study. *Earth Planet Sci Lett* 304:113–120
- Li XF, Zhao H, Tang M, Liu Y (2009) Theoretical prediction for several important equilibrium Ge isotope fractionation factors and the geological implication. *Earth Planet Sci Lett* 287:1–11
- Liu Y (2013) On the test of a new volume variable cluster model method for stable isotopic fractionation of solids: Equilibrium Mg isotopic fractionations between minerals and solutions. Goldschmidt 2013 Conference Abstracts 1632
- Liu Y, Tossell JA (2005) Ab initio molecular orbital calculations for boron isotope fractionations on boric acids and borates. *Geochemica et Cosmochimica Acta*. 69:3995–4006
- Liu Q, Tossell JA, Liu Y (2010) On the proper use of the Bigeleisen-Mayer equation and corrections to it in the calculation of isotopic fractionation equilibrium constants. *Geochemica et Cosmochimica Acta* 74:6965–6983
- McIntosh GJ (2012) A theoretical kinetic model of the temperature and pH dependent dimerization of orthosilicic acid in aqueous solution. *Phys Chem Chem Phys* 14:996–1013
- McIntosh GJ, Swedlund PJ, Söhnle T (2011) Experimental and theoretical investigations into the counter-intuitive shift in the antisymmetric v (Si–O) vibrational modes upon deuteration of solvated silicic acid (H_4SiO_4). *Phys Chem Chem Phys* 13:2314–2322
- Nangia S, Garrison BJ (2008) Reaction rates and dissolution mechanisms of quartz as a function of pH. *J Phys Chem A* 112:2027–2033
- Okamoto A, Tsuchiya N (2009) Velocity of vertical fluid ascent within vein-forming fractures. *Geology* 37:563–566
- Opfergelt S, Delmelle P (2012) Silicon isotopes and continental weathering processes: assessing controls on Si transfer to the ocean. *CR Geosci* 344:723–738
- Pokrovski GS, Schott J, Farges F, Hazemann J (2003) Iron (III)-silica interaction in aqueous solution: insights from X-ray absorption fine structure spectroscopy. *Geochemica et Cosmochimica Acta* 67:3359–3373
- Rastsvetaeva RK, Chukanov NV, Zadov AE (2009) Refined structure of afwillite from the northern Baikal region. *Crystallogr Rep* 54:418–422
- Rustad JR, Casey WH, Yin Q-Z, Bylaska EJ, Felmy AR, Bogatko SA, Jackson VE, Dixon DA (2010) Isotopic fractionation of Mg^{2+} (aq), Ca^{2+} (aq), and Fe^{2+} (aq) with carbonate minerals. *Geochemica et Cosmochimica Acta* 74(22):6301–6323
- Schauble EA (2004) Applying stable isotope fractionation theory to new systems. *Rev Miner Geochem* 55:65–111
- Swedlund PJ, Miskelly GM, McQuillan AJ (2010) Silicic acid adsorption and oligomerization at the ferrihydrate–water interface: interpretation of ATR-IR Spectra based on a model surface structure. *Langmuir* 26:3394–3401
- Urey HC (1947) The thermodynamic properties of isotopic substances. *J Chem Soc (London)* 85:562–581
- Van den Boorn SHJM, van Bergen MJ, Vroon PZ, de Vries ST, Nijman W (2010) Silicon isotope and trace element constraints on the origin of ~ 3.5 Ga cherts: implications for Early Archean marine environments. *Geochemica et Cosmochimica Acta* 74:1077–1103
- Wong MW (1996) Vibrational frequency prediction using density functional theory. *Chem Phys Lett* 256:391–399
- Zhang ST, Liu Y (2014) Molecular-level mechanisms of quartz dissolution under neutral and alkaline conditions in the presence of electrolytes. *Geochem J* 48:189–205
- Ziegler K, Chadwick OA, Brzezinski MA, Kelly EF (2005a) Natural variations of $\delta^{30}\text{Si}$ ratios during progressive basalt weathering, Hawaiian Islands. *Geochemica et Cosmochimica Acta* 69:4597–4610
- Ziegler K, Chadwick OA, White AF, Brzezinski MA (2005b) $\delta^{30}\text{Si}$ systematics in a granitic saprolite, Puerto Rico. *Geology* 33:817–820